so that the results represented in Fig. 4 retain their value.

In conclusion, it should be noted that insertion of a sharp boundary between zones 1 and 2 as well as the approximation $R_3 = 1$ will increase the reflection coefficient R. Hence, the computed value of the energy flux S_{10} should be considered an upper bound.

LITERATURE CITED

1. V. I. Aleksandrov, V. V. Osiko, et al., "New method of obtaining refractory single-crystals and melts of ceramic materials," Vestn. Akad. Nauk SSSR, No. 12 (1973).
2. A. G. Merzhanov, V. A. Raduchev, and É. N. Rumanov, "Thermal melting waves and dielectric crystallization," Dokl. Akad. Nauk SSSR, 253, No. 2 (1980).
3. Yu. P. Raizer, "High-pressure microwave discharge propagation," Zh. Eksp. Teor. Fiz., 61, No. 1 (1971).
4. I. E. Poyurovskaya, M. I. Tribel'skii, and V. I. Fisher, "On the ionization wave sustainable by powerful monochromatic radiation," Zh. Eksp. Teor. Fiz., 82, No. 6 (1982).
5. Ya. B. Zel'dovich, "On the theory of flame propagation," Zh. Fiz. Khim., 22 (1948).
6. L. D. Landau and E. M. Lifshits, Electrodynamics of Continuous Media [in Russian], Fizmatgiz, Moscow (1957).
7. F. V. Bunkin, N. A. Kirichenko, and B. S. Luk'yanchuk, "Thermochemical phenomena stimulated by laser radiation," Izv. Akad. Nauk SSSR, Ser. Fiz., 45, No. 6 (1981).
8. A. G. Merzhanov, É. N. Rumanov, and B. I. Khaikin, "Multizone combustion of condensed systems," Zh. Prikl. Mekh. Tekh. Fiz., No. 6 (1972).

MOTION OF A CURRENT-CARRYING PLASMA SHELL IN A RAREFACTION WAVE

V. S. Komel'kov, A. P. Kuznetsov, and A. S. Pleshanov

UDC 533.9.07

The paper is an extension of the research of [1, 2]. In [2] it was shown, both experimentally and theoretically, that a plasma shell generated by a coaxial accelerator can also be accelerated beyond the limits of the coaxial section. The existence of limits to such acceleration was also indicated there. It turned out that high parameters of the accelerated plasma can be obtained (at currents of order 1 MA) only when the gas filling the accelerator has a relatively low density (a number of hydrogen atoms $n \leqslant 10^{17}$ 1/cm^3). For the experiment described in [1, 2] the interelectrode space must be filled with a gas having a density an order of magnitude greater than that at which it is possible to obtain a high-temperature plasma. A conflict arises between the demands for performing the experiment and the conditions for obtaining high-parameter plasma formations. This conflict can be eliminated, in our view, if the plasma is accelerated in a rarefaction wave propagating opposite to the motion of the plasma shell. With the appropriate synchronization of the motion of the plasma and the rarefaction wave one can assure the development of a discharge and the formation of a shell in a sufficiently dense gas, while the plasma acceleration occurs, as in [2, 3], beyond the cut of the accelerator in the considerably less dense medium formed by the rarefaction wave.

The present work was devoted to a numerical investigation of the possibilities of such plasma acceleration. One of the possible schemes for it is presented in Fig. 1, where 1 is the coaxial accelerator with energy storage, 2 is the accelerator chamber, 3 is a diaphragm that opens, and 4 is the evacuated section. In such an apparatus the process develops as follows. The coaxial accelerator ejects into the accelerator chamber a plasma cluster which is formed under the action of the current flowing into the shell (Fig. 2). At a certain instant the diaphragm is opened and a rarefaction wave is formed, in which the current-carrying shell to be accelerated moves.

Statement of the Problem

We consider only the process taking place beyond the cut of the coaxial plasma accelerator. The plasma emitted from the accelerator consists of an axisymmetric shell formed by the

Moscow. Translated from Zhurnal Prikladnoi Mekhaniki i Tekhnicheskoi Fiziki, No. 1, pp. 13-18, January-February, 1985. Original article submitted October 31, 1983.

0021-8944/85/2601-0010$09.50

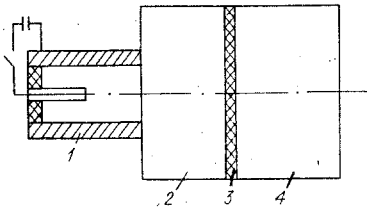

Fig. 1

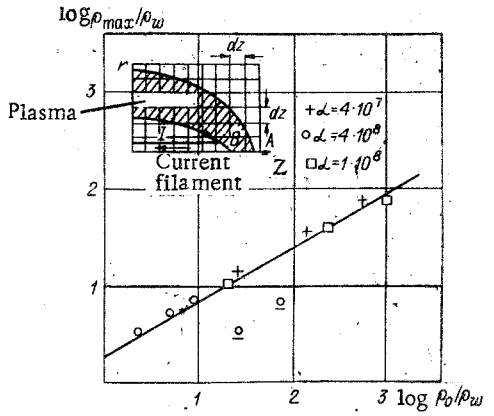

Fig. 2

plasma ejected from the accelerator and the plasma formed behind the shock wave propagating through the gas surrounding the accelerator. Inside the shell there is a current filament (this is confirmed experimentally [2-4]) connecting the inner coaxial electrode with the shell. The circuit is closed by the plasma itself. As in [2], the plasma can be considered as perfectly conducting and quasineutral. A schematic picture of the phenomenon being calculated is presented in the upper corner of Fig. 2.

The equations describing the process are purely hydrodynamic,

$$\frac{\partial u}{\partial t}+u\frac{\partial u}{\partial r}+v\frac{\partial u}{\partial z}+\frac{1}{\rho}\frac{\partial p}{\partial r}=0,$$

$$\frac{\partial v}{\partial t}+u\frac{\partial v}{\partial r}+v\frac{\partial v}{\partial z}+\frac{1}{\rho}\frac{\partial p}{\partial z}=0,$$

$$\frac{\partial \varepsilon}{\partial t}+u\frac{\partial \varepsilon}{\partial r}+v\frac{\partial \varepsilon}{\partial z}+\frac{p}{\rho}\left[\frac{1}{r}\frac{\partial (ur)}{\partial r}+\frac{\partial v}{\partial z}\right]=0,$$

where r and z are the radial and axial coordinates, respectively; u and v, radial and axial velocity components; ρ, density; p, pressure; ε, specific internal energy. As in [2], we used tables of thermodynamic functions of hydrogen and a modified numerical method of particles in cells.

Initial and Boundary Conditions

At the initial time the plasma cluster was assumed to be a disk of plasma compressed in the shock wave. The parameters of the plasma were determined by the current and the initial gas density in the accelerator and were calculated in accordance with the experimental data and the procedure described in [2]. The rarefaction wave was assumed to be plane at the initial time. Its front lay at a distance of four cells of the calculation grid from the accelerator cut and the critical cross section of the wave had the coordinate z = 10 cells. The "tail" of the wave extended beyond the edge of the calculation field. Conditions of the "rigid-wall" type were assigned at the coordinate surfaces r = 0 (the z axis) and z = 0 (the plane of the coaxial cut). In cells adjacent to the accelerator cut the plasma flux was kept constant until all the plasma contained in the accelerator had flowed out.

The shell configuration is formed starting with this time. The cavity of the shell is acted on by a magnetic pressure p_m, determined by the current I flowing through the filament and the distance r from the z axis,

$$p_m=\frac{\mu_0}{2}\left(\frac{I}{2\pi r}\right)^2,$$

where μ_0 is the magnetic permeability of a vacuum. As in [2], the pressure in the current filament was found from the condition of equilibrium, while its diameter was taken as 5 mm. The step of the calculation grid was set at 10^{-2} m along both coordinates. The time step was determined by the Courant stability condition.

Results of the Calculations

We calculated three variants, differing in the value of the current (1 or 2 MA) and the initial hydrogen pressure p_0 (10^4 or 10^5 Pa). It is convenient to characterize each variant by the parameter $\alpha = I^2/p_0$, A^2/Pa. This quantity determines the initial intensity of the

shock wave and allows one to make a comparison with the variants of [2], where it also figures. Three values of α were adopted in the variants under discussion here: $4 \cdot 10^8$ (I = 2 MA, $p_0 = 10^4$ Pa), $4 \cdot 10^7$ (I = 2 MA, $p_0 = 10^5$ Pa), and 10^8 (I = 1 MA, $p_0 = 10^4$ Pa). As in [2], principal attention was devoted to the axial region of the shell in the investigation. The formation of a high-temperature and relatively dense plasma was expected just here.

Figures 2-5 illustrate the results of the calculations. In Fig. 4 we present the trajectories of motion of two characteristic points of the shell, A (Z_{ex}, 0) and B (Z_{in}, 0), obtained for variant 1. Here Z_{ex} is the z coordinate reached by the shock wave propagating along the axis of symmetry; Z_{in} is the z coordinate reached by the point of the cavity located on the axis of symmetry. The trajectories of motion of these same points from [2] are presented in Fig. 4 for comparison (lines not marked by crosses). The considerably altered character of the motion of these points is noted. From the first, point A moves noticeably faster in the rarefaction wave than in the uniform medium. For quite a long time the trajectory of point B when moving in the rarefaction wave does not differ from the trajectory of this point moving in a uniform medium. This is understandable. The trajectory of point A is the trajectory of a shock wave generated by a moving piston, and the fact of its acceleration as the shell moves in the rarefaction wave is explained by the fact that as the shock wave advances, it emerges into ever more rarefied regions of space. This fact accords with the results of a solution of the one-dimensional, self-similar problem of the propagation of a shock wave in an atmosphere with a density decreasing in accordance with a power law [5]. The following can be said about the trajectory of point B. Its motion is determined to a considerable extent by the amount of plasma in its vicinity. And this amount itself depends on the velocity of radial plasma flow and initially it is practically the same both in the case of the efflux of the shell in a uniform medium and in the case of efflux in a rarefaction wave. It is determined by the initial gas density inside the accelerator and by the value of the current. With time the radial flux in the vicinity of point B for efflux into a rarefaction wave starts to exceed the radial flux for efflux into a uniform medium (the "information," supplied by the C characteristics for the periphery of the shell, that the resistance of the medium is considerably lower due to the presence of the rarefaction wave than in its absence, reaches the axial region), the amount of material here decreases considerably, and the velocity of point B grows. It is important to note, however, that in contrast to the motion of a shell in a uniform medium, the velocity of motion of point A exceeds the velocity of motion of point B: As it propagates through a medium with a decreasing density the shock wave is separated more and more from the piston.

Density profiles pertaining to different times for variant 1 are shown in Fig. 3. The times were determined by the position of point A relative to the rarefaction wave. The profiles were taken along the line AB, i.e., along the axis of symmetry. Here we also show the density distribution in the rarefaction wave itself, which pertains to the initial time. We note that the profile of the shell varies insignificantly over the time of its passage through the rarefaction wave in view of the brevity of the process, and for purposes of illustration it is sufficient to work with distributions of the gas parameters in the rarefaction wave pertaining just to the initial time.

We were able to obtain very interesting results in an analysis of the degree of compression of the material in the axial region. Figure 2 represents the dependence of the quantity $K = \log(\rho_{max}/\rho_w)$, characterizing the degree of compression, on the variable $x = \log(\rho_0/\rho_w)$. Here ρ_{max} is the maximum value of the shell density (reached at the point B); ρ_w is the density of the medium in the rarefaction wave at the point reached by the point B at the given time; ρ_0 is the density of the medium undisturbed by the rarefaction wave. As seen from Fig. 2, the logarithmic coefficient of maximum compression of material in the shell is a linear function of the logarithmic "distance" of the point of maximum compression from the front of the rarefaction wave:

$$K = 0.55x + 0.3. \quad (1)$$

The same relation can also be expressed in terms of absolute quantities:

$$\rho_{max} = 2\rho_0^{0.55}\rho_w^{0.45} \approx 2\sqrt{\rho_0\rho_w}.$$

The relation (1) satisfactorily describes all the calculated variants and is valid for almost all times. Only the points of the variant $\alpha = 4 \cdot 10^8$ pertaining to later times do not lie on the straight line 1. These points are underlined in Fig. 2.

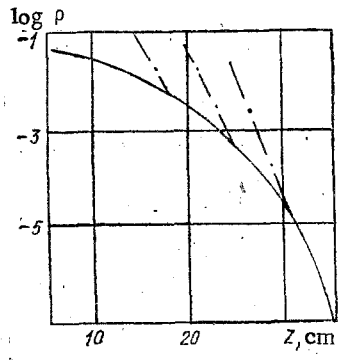

Fig. 3

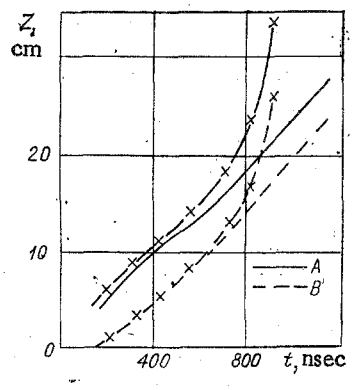

Fig. 4

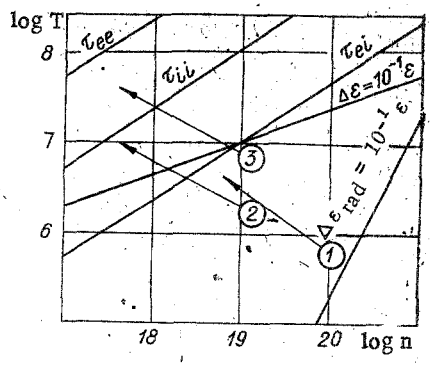

Fig. 5

In comparing the results obtained and the results of [2] we can note that acceleration in a rarefaction wave enables one to increase the velocity of plasma flow in the axial region and the plasma temperature by 5-8 times for a decrease in density by 20-30 times. The parameters of the accelerated plasma had the following absolute values (in the numerical order of the variants): $T = 4\cdot10^6$, 10^7°K; $v = 10^6$, $2\cdot10^6$ m/sec; $n = 6\cdot10^{18}$, $3.8\cdot10^{17}$ 1/cm^3.

An important fact for the phenomenon as a whole is that the technique of plasma acceleration in a rarefaction wave, by allowing one to initiate the discharge in a very dense medium and providing the necessary conditions for the formation of a shell, makes it possible to achieve those parameters of the accelerated plasma which could be obtained for acceleration into a medium of constant density an order of magnitude lower than ρ_0. In other words, acceleration in a rarefaction wave requires currents two to three times lower to obtain the same plasma parameters as acceleration into a medium of constant density (equal to ρ_0).

Physical Basis for the Adopted Shell Model

The calculated results presented above were obtained under the following assumptions about the properties of the plasma: a) The plasma is in equilibrium; b) the influence of radiation and electronic heat conduction distorts the internal energy distribution insignificantly. Before proceeding to a discussion of these questions, we note that the characteristics required for estimates of the properties of the plasma have a power-law dependence on its temperature T and density n [5]:

$$f = cT^{\beta} n^{\delta}. \qquad (2)$$

Here f is a characteristic of the plasma (time of establishment, radiation density, etc.). This facilitates the analysis and permits the clear illustration of the results obtained. For this purpose, points characterizing the state of the plasma during its efflux into a medium with a constant density, numbered by the increase in α, are plotted in Fig. 5 in logarithmic n–T coordinates. The arrows show the states at which the plasma arrives after passage through the rarefaction wave. The straight lines plotted in Fig. 5 in accordance with (2) define the boundaries of the region where one or another assumption about the limiting value of the characteristic f is correct.

The times of establishment of component-by-component equilibrium (electronic τ_{ee} and τ_{ii}) and of intercomponent equilibrium (τ_{ei}) are characteristics of the plasma equilibrium. Keeping in mind that $\beta = 1.5$ and $\delta = -1$ in (2), while the characteristic time of the process is $\tau = 10^{-7}$ sec, we obtain the equations for the respective boundaries:

$$\lg T = 0.67 \lg n - 3.6 \text{ for } \tau_{ee},$$
$$\lg T = 0.67 \lg n - 4.67 \text{ for } \tau_{ii},$$
$$\lg T = 0.67 \lg n - 5.75 \text{ for } \tau_{ei}.$$

It is seen from Fig. 5 that an equilibrium (one-fluid) plasma occurs absolutely only for variant 1. Variant 2 is in equilibrium, while variant 3 is almost in equilibrium, relative to the establishment of component-by-component equilibrium. The fact that intercomponent equilibrium is not established in these variants cannot significantly affect the results of the calculations. The point is that the calculation procedure does not deal directly with the temperature but operates with the internal energy, enabling one (when component-by-component equilibrium is present) to correctly determine both the state of the plasma and its dynamics.

Thus, we can say that the one-fluid model of an equilibrium plasma proved to be a fully satisfactory assumption for the given value of τ.

Let us estimate the influence of electronic heat conduction. From the heat-conduction equation we find that the heat losses $\Delta\varepsilon$ through the surface $S = l^2$ for given characteristic values of the size l, the maximum temperature T, and the time τ are expressed as

$$\Delta\varepsilon = \bar{\varkappa}(T/l)l^2\tau, \tag{3}$$

where $\bar{\varkappa}$ is the average value of the coefficient of thermal conductivity. Substituting into (3) the value of $\bar{\varkappa}$ from [5] and taking $l = 0.1$ and $\tau = 10^{-7}$ sec, we obtain

$$\Delta\varepsilon = 3.5\cdot10^{-13}T^{7/2}\ \text{erg}. \tag{4}$$

In turn, the internal energy of the volume l^3 is

$$\varepsilon = \frac{2nkT}{\gamma-1}l^3 = 10^{-13}nT. \tag{5}$$

To justify neglecting the influence of electronic heat conduction it is necessary that $\Delta\varepsilon \ll \varepsilon$. Assigning a tenfold excess of ε over $\Delta\varepsilon$ and combining (4) and (5), we obtain

$$\lg T = 0.4\lg n - 0.62.$$

An analysis of the location of the points characterizing the state of the plasma for the different variants shows that allowance for electronic heat conduction is unimportant for variant 1. This conclusion is also valid for variant 2, since states for which this influence becomes appreciable are reached only in the last stage of efflux, and the characteristic time of the process can be reduced by several times compared with the value of $\tau = 10^{-7}$ sec used in the estimates. As for variant 3, its results are incorrect, strictly speaking. The actual state of the plasma will be such that its temperature hardly exceeds 10^7°K. The discovered flow anomaly might be of interest, but the low reliability of the results, obtained without allowance for electronic heat conduction, prevents us from paying it any significant attention.

To answer the question of the influence of radiation on the results obtained, we compare the internal energy density with the radiation flux density. For a photon mean free path $l_{ph} > l$ (just this regime is characteristic for all the calculated variants) the boundary of the region where the radiation density $\Delta\varepsilon_{rad}$ is much less than the internal energy density is determined by the relation [5]

$$\Delta\varepsilon_{rad} = 1{,}42\cdot10^{-27}n^2T^{1/2}\tau \ll 2nkT/(\gamma-1).$$

After transformations, and assigning a tenfold excess of ε over $\Delta\varepsilon_{rad}$, we have

$$\lg T = -34.64 + 2\lg n. \tag{6}$$

The region where the assumption made is legitimate lies above the straight line (6) in Fig. 5. It is seen that none of the calculated variants need refinement in connection with the allowance for radiation.

In summing up the foregoing, we can say that the adopted shell model works with sufficient validity under the assumptions made.

The above numerical experiments showed that the acceleration of a plasma shell in a rarefaction wave increases the resources of the accelerator, permitting confidence in obtaining pulsed streams of high-temperature ($T \gtrsim 10^7$°K) and relatively dense ($n = 10^{17}$ 1/cm^3) plasma. Evidently, the data obtained can also be of interest for the investigation of processes in accelerators with a pulsed gas supply, since acceleration in them is also accompanied by the presence of a rarefaction wave traveling opposite to the plasma being accelerated.

In addition, the analysis of plasma efflux in a rarefaction wave can prove useful for clarifying the mechanism of acceleration of elementary particles in processes analogous to those which occur at the surface of a star when a strong shock wave arrives at it [6] or in the efflux of a laser plasma from the surface of a target [7].

LITERATURE CITED

1. V. S. Komel'kov, A. P. Kuznetsov, et al., "Efflux of a plasma current shell," Zh. Prikl. Mekh. Tekh. Fiz., No. 5 (1978).

2. V. S. Komel'kov, A. P. Kuznetsov, et al., "Dynamics of a plasma shell with an external current," Zh. Prikl. Mekh. Tekh. Fiz., No. 2 (1982).
3. V. S. Komel'kov and V. I. Modzolevskii, "A coaxial accelerator for dense plasma," Fiz. Plazmy, 3, No. 5 (1977).
4. V. I. Vasil'ev, V. S. Komel'kov, et al., "A stable dynamic current filament," Zh. Tekh. Fiz., 30, 756 (1960).
5. Ya. B. Zel'dovich and Yu. P. Raizer, Physics of Shock Waves and High-Temperature Hydrodynamic Phenomena, Academic Press, New York (1967).
6. S. A. Colgate and M. H. Jonson, "Hydrodynamic origin of cosmic rays," Phys. Rev. Lett., 5, No. 6 (1960).
7. N. G. Basov, S. V. Bobashev, et al., "Spectrometric observations of multiply charged ions of megavolt energies in a laser plasma," Pis'ma Zh. Eksp. Teor. Fiz., 36, No. 7 (1982).

MAGNETOPLASTICITY OF MAGNETIZABLE MEDIA

N. D. Slatinskii and I. E. Tarapov

UDC 537.84:539.374

An important problem in modern mechanics is the study of the behavior of continuous media in strong electromagnetic fields [1]. Here media with strongly manifested magnetic properties are of great interest, because in such media the interaction of the medium with the electromagnetic field through the ponderomotive forces and energy flow from the field into the material, owing to the magnetization, plays an important role.

Magnetoplastic flows of magnetizable media are realized in elements of engineering structures, operating in magnetic fields, which create pressures close to the yield point of the magnetic material [2]. The study of such flows is of interest for powder metallurgy and high-pressure metal working [3]. It is expected that the magnetization effect is important in materials formed by sintering of ferromagnets with other metals.

The basic system of equations describing magnetoplasticity, ignoring the effects of magnetization, is derived in [4]. The basic equations of motion of magnetizable media are derived in [5].

We assume that the processes studied in the incompressible and perfectly conducting medium are quasistationary and that the magnetization is reversible. To describe plastic flows of magnetizable media in an electromagnetic field, starting from [4, 5] we obtain a closed system of equations in the following form:

$$\nabla_k v^k = 0; \tag{1}$$

$$\rho dv_i/dt = \nabla_k p^{ik}; \tag{2}$$

$$\rho T \frac{d}{dt}\left(s + \frac{\mu_0}{\rho}\int_0^H \left(\frac{\partial M}{\partial T}\right)_{\rho,H} dH\right) = P^{0*}_{ik} v^{ik} + \operatorname{div}(\lambda \nabla T); \tag{3}$$

$$\nabla_k B^k = 0; \tag{4}$$

$$\partial \mathbf{B}/\partial t = \operatorname{curl}[\mathbf{v}, \mathbf{B}]; \tag{5}$$

$$P^{0*}_{ik} = \eta v_{ik}; \tag{6}$$

$$\frac{1}{2} P^{0*}_{ik} P^{0*ik} = k^2. \tag{7}$$

Here $P_{ik} = P^0_{ik} + P^H_{ik}$ is the total stress tensor, and $P^H_{ik} = -g_{ik}\left(\mu_0 \frac{H^2}{2} + \mu_0 \int_0^H \left(M - \rho\left(\frac{\partial M}{\partial \rho}\right)_{T,H}\right) dH\right) +$ $H_i B_k$ is its magnetic part; ρ, v, T, and s are the density, velocity, temperature, and entropy of the medium, respectively; **H** and **B** are the magnetic field intensity and induction; λ is the coefficient of the thermal conductivity; the asterisk indicates the divisor of the stress

Kharkov. Translated from Zhurnal Prikladnoi Mekhaniki i Tekhnicheskoi Fiziki, No. 1, pp. 18-22, January-February, 1985. Original article submitted November 24, 1983.

